Journal of Catalysis 376 (2019) 248–257

Contents lists available at ScienceDirect

Journal of Catalysis

journal homepage: www.elsevier.com/locate/jcat

Kinetic analysis and reaction mechanism for anisole conversion over zirconia-supported molybdenum oxide

Manish Shetty [1], Eric M. Anderson, William H. Green *, Yuriy Román-Leshkov *

Department of Chemical Engineering, Massachusetts Institute of Technology, Cambridge, MA 02139, USA

ARTICLE INFO

Article history:
Received 18 December 2018
Revised 1 June 2019
Accepted 30 June 2019

Keywords:
Hydrodeoxygenation (HDO)
Alkylation
Kinetics
Anisole
Co-feed
Bifunctional catalysis
Molybdenum oxide

ABSTRACT

Gas-phase catalytic conversion of anisole and its reaction intermediates was studied over a 10 wt% MoO_3/ZrO_2 catalyst at temperatures between 553 and 633 K and H_2 partial pressures (P_{H2}) ≤ 1 bar. Benzene, phenol, cresol and methyl anisole were identified as the primary products from the hydrodeoxygenation (HDO), hydrogenolysis, intra- and intermolecular alkylation of anisole, respectively. The anisole to benzene conversion featured a first-order dependence with respect to P_{H2}, while the conversion of phenol to benzene and m-cresol to toluene, showed P_{H2} and $P_{oxygenate}$ reaction orders of 1/2 and zero, respectively. A kinetic model showed that although the secondary pathway of phenol HDO to benzene has a rate constant ~3 times higher than that for the HDO of anisole to benzene, the anisole HDO pathway is dominant at low anisole conversions. Apparent orders of ~½ with $P_{oxygenate}$ for anisole hydrogenolysis and alkylation to form phenol, cresol, and methyl anisole implied the existence of different active sites than those responsible for HDO. Co-feed studies with H_2O, pyridine, and di-tert butyl pyridine (DTBP) indicated that the active-sites responsible for HDO have a Lewis acid character that is associated with oxygen vacancies and that is distinct from the nature of sites responsible for hydrogenolysis and alkylation. Accordingly, co-feeding CH_3OH resulted in increased phenol alkylation rates to form alkylated cresols along with inhibition of phenol to benzene HDO rates. A three-site model was proposed to unify the HDO, hydrogenolysis, and alkylation reactivity data obtained from the kinetic and co-feed studies.

1. Introduction

The development of catalysts for the hydrodeoxygenation (HDO) of lignin-derived phenolic compounds obtained from the catalytic fast pyrolysis (CFP) and reductive catalytic fractionation (RCF) of biomass is an important step in the valorization of biomass into value-added chemicals and fuels [1–17]. These compounds, including eugenol, syringol, and guaiacol, contain both $C_{aromatic}$-OH and $C_{aromatic}$-OCH_3 bonds that are cleaved during the HDO process [11,18]. The fate of the reaction products hinges on effective catalyst and reactor design, which in turn requires fundamental insights into the chemical kinetics and the nature of active sites responsible for bond activation [19–25]. Recently, Román-Leshkov and coworkers have demonstrated that bulk and supported MoO_3 catalysts are highly effective at the HDO of lignin-derived phenolics into aromatic hydrocarbons at mild conditions (593 K and H_2 partial pressures ≤1 bar) without ring-saturation [26–28]. These MoO_3-based catalysts were shown to be a promising alternative to zeolites for the upgrading of bio-oils obtained from the CFP of lignocellulosic biomass [29–32]. Shetty et al. demonstrated that anisole conversion on MoO_3/ZrO_2 catalysts formed HDO (e.g., benzene and toluene), hydrogenolysis (e.g., phenol) and alkylation (e.g., methylated cresols and anisoles) products [33]. While the product distributions and the impact of MoO_3 loading on the reactivity towards HDO and alkylation were reported, detailed information on the reaction kinetics and HDO mechanism were not elucidated for supported MoO_3 catalysts.

Herein, we report a detailed investigation of the reaction network, kinetics, and nature of active sites for the conversion of anisole over a 10 wt% MoO_3/ZrO_2 catalyst. The reaction network was determined by varying the catalyst contact times to determine primary, secondary and higher-order products. Next, the kinetics for anisole conversion to benzene, phenol, cresol and methyl anisole, as well as the HDO of the intermediates phenol and m-cresol to benzene and toluene, respectively, were studied on supported MoO_3 catalysts over a temperature range of 553–633 K.

* Corresponding authors.
E-mail addresses: whgreen@mit.edu (W.H. Green), yroman@mit.edu (Y. Román-Leshkov).
[1] Present address: Institute of Integrated Catalysis (IIC), Pacific Northwest National Laboratory (PNNL), 902 Battelle Boulevard, Richland, WA 99354, USA.

https://doi.org/10.1016/j.jcat.2019.06.046
0021-9517/

The nature of the active sites was probed with the aid of control reactions, co-feed studies with pyridine, water (H_2O), methanol (CH_3OH), and di-tert butyl pyridine (DTBP). Lastly, a macrokinetic model involving oxygenate and H_2 activation over three distinct sites was proposed to described the observed reactivity data.

2. Materials and methods

2.1. Materials and reactivity measurements

The 10 wt% MoO_3/ZrO_2 catalyst and the ZrO_2 support were synthesized with procedures described in previous reports [28]. Bulk MoO_3 (99.97% trace metals basis, Sigma Aldrich) was used without any purification or pretreatment. Reactivity studies were carried out in the vapor-phase in a packed-bed, down-flow reactor. The reactor consisted of a stainless-steel tube (0.95 cm OD, with wall thickness of 0.089 cm) mounted in a single-zone furnace (Applied Test Systems, Series 3210, 850 W/115 V). The temperature was controlled by a temperature controller (Digi-Sense, model 68900-10) connected to a K-type thermocouple (Omega, model TJ36-CAXL-116u) mounted downstream in direct contact with the catalyst bed. The catalyst was pelletized between 100 and 140 mesh, mixed with inert α-Al_2O_3 diluent (100–200 mesh, total 1 g), and packed between two layers of α-Al_2O_3 (1.5 g each) in the middle of the furnace. Prior to the reaction, the reactor temperature was ramped at a rate of ~6 K min^{-1} under N_2 until reaching the reaction temperature (553–613 K). Next, an oxygenated feed (anisole, phenol solution in mesitylene or m-cresol solution in cyclohexane) was delivered into the reactor via a capillary tube connected to a syringe pump (Harvard Apparatus, model 703005) and mixed with H_2 gas at the inlet of the reactor. Catalyst contact times were changed by adjusting the flow rates of the oxygenate feed to vary the weight hourly space velocity (WHSV), defined with respect to the equivalent mass of MoO_3 loaded [33]. Typically, flow rates of the oxygenate feed ranged between 100 and 400 μl h^{-1}. The mass of equivalent MoO_3 was computed as the product of MoO_3 loading (10 wt%) and the total mass of catalyst loaded.

The reactor effluent lines were heated to 523 K to prevent condensation. The effluents were analyzed and quantified via an online gas chromatograph (GC) fitted with a DB-5 column (Agilent, 30 m × 0.25 mm ID × 0.25 μm) and equipped with a mass selective detector for identification (MSD, Agilent Technologies, model 5975C) and a flame ionization detector (FID, Agilent Technologies, model 7890 A) for quantification. The GC parameters used for analysis were as follows: detector temperature 573 K, injector temperature 548 K, split ratio 1:20. The initial and final oven temperatures were 323 and 523 K, with a ramp of 10 K min^{-1}.

The following equations were used to quantify experimental data. The carbon balances were typically above 95%, (calculated by comparing the total carbon moles of reaction products) as shown in Fig. S1a. Our previous reports have shown that carbon lost as coke is insignificant under the reaction conditions used in this study [28]. Hence, the selectivity and yield were defined based on the GC observable products.

$$Conversion(C-mol\%) = \frac{Carbon\ moles\ of\ reactant\ consumed}{Carbon\ moles\ of\ reactant\ fed} \times 100 \quad (1)$$

$$Selectivity(C-mol\%) = \frac{Carbon\ moles\ in\ product}{Total\ carbon\ moles\ in\ products} \times 100 \quad (2)$$

$$Yield(C-mol\%) = \frac{Carbon\ moles\ in\ product}{Carbon\ moles\ of\ reactant\ fed} \times 100 \quad (3)$$

The kinetic experiments were performed at differential conditions (<15% conversion) on a C-mol% basis (unless otherwise specified). The kinetic studies for determining reaction orders for the HDO of anisole, phenol, and m-cresol were performed on 10 wt% MoO_3/ZrO_2 and bulk MoO_3 catalysts, while the kinetic studies for the hydrogenolysis and alkylation reactions were performed on the bare ZrO_2 support and the 10 wt% MoO_3/ZrO_2 catalyst. The reported reaction rates for 10 wt% MoO_3/ZrO_2 and ZrO_2 were obtained from steady-state data, while for bulk MoO_3 it was obtained from the maximum rate after the induction period. As discussed in previous reports, bulk MoO_3 undergoes an induction period before reaching peak reactivity followed by gradual deactivation [27,28]. The apparent kinetic orders with respect to anisole and H_2 were obtained by varying their partial pressures from 0.0049 to 0.0147 bar, and 0.2508–1.0032 bar, respectively. At P_{H2} < 1.0032 bar, the P_{Total} was 1.013 bar with N_2 as the balance gas. Solutions of 50 wt% in mesitylene and 40% in cyclohexane were used for phenol and m-cresol, respectively (unless mentioned otherwise). Mesitylene and cyclohexane did not react on contact with the catalyst. The activation energy barriers were calculated by varying the reaction temperatures between 573 and 613 K (unless mentioned otherwise) for 10 wt% MoO_3/ZrO_2 and 553–613 K for bulk MoO_3.

2.2. Co-feed experiments

The co-feed experiments were carried out with water (H_2O), methanol (CH_3OH), pyridine and ditertbutyl pyridine (DTBP). Pyridine and DTBP were introduced in a solution with anisole from a different syringe pump (Harvard apparatus, model 703310) while maintaining the partial pressure of anisole ($P_{Anisole}$) at a constant value. The partial pressure of both pyridine and DTBP was ~0.0015 bar·H_2O or CH_3OH were introduced as a saturated feed by bubbling H_2 through liquid H_2O or CH_3OH while maintaining $P_{Anisole}$ at a constant value, with P_{H2O} and P_{CH3OH} values of 0.032 and 0.16 bar, respectively, as determined by vapor pressure data at room temperature.

2.3. Fourier transform infrared (FTIR) spectroscopy

FTIR spectra of the 10 wt% MoO_3/ZrO_2 catalyst were acquired from 4000 to 400 cm^{-1} using a Bruker Vertex 70 spectrophotometer by averaging 64 scans at a 2 cm^{-1} resolution. Samples were pressed into 7 mm diameter self-supporting pellets and placed in a Harrick high temperature transmission cell equipped with KBr windows. Samples were calcined *in situ* under flowing dry air (50 ml min^{-1}), with a temperature ramp of 5 K min^{-1} to 773 K, and held at 773 K for 1 h. After the cell was cooled to room temperature, dynamic vacuum of ~0.1 Pa was established and a reference spectrum of the bare material was acquired. Under a static vacuum, the cell was progressively dosed with pyridine and/or DTBP vapor until physisorption peaks were observed. After overnight evacuation at room temperature, spectra were collected as the temperature was increased in 50 K increments (rate 5 K min^{-1}) up to 623 K, and then cooled to room temperature. Similar acquisition protocols were used after H_2 treatment at 593 K.

2.4. Ammonia-temperature programed desorption (NH_3-TPD)

NH_3-TPD was performed in a quartz U-tube reactor setup mounted in an insulated single-zone furnace (550 W/115 V, Carbolite GTF 11/50/150B) connected to an online mass spectrometer (MS, HIDEN Analytical HPR-20/QIC). 100 mg of catalyst (60–100 mesh) was loaded into a U-tube packed between quartz wool. The catalyst bed was in contact with a K-type thermocouple (Omega, model TJ36-CAXL-116u) that was connected to a temper-

ature controller. The catalyst was calcined in O_2 at 100 ml min^{-1} at 773 K for 2 h at a ramp rate of 5 K min^{-1} and cooled under 1% Ar in He to 373 K (100 ml min^{-1}). The catalyst was exposed to several pulses of NH_3 totaling ~10 ml of NH_3 at STP. The catalyst was purged with 1% Ar in He for 1 h at 373 K. The sample was then heated to 823 K (10 K min^{-1}) and held for 30 min at 823 K. The evolved NH_3 was monitored with MS by tracking the m/z = 17 fragment. The MS response was calibrated for each ammonia pulse prior to the analysis. The acidity was estimated assuming a ratio of acid-site/NH_3 = 1.

2.5. Reactor model

We assumed isothermal operation of a plug flow reactor with negligible pressure drop across the catalyst bed. A packed bed reactor (PBR) model was employed (see Eq. (4)):

$$\frac{dF_i}{dW} = R_i \tag{4}$$

$$\text{with initial condition of } F_i = F_{i,0} \text{ at } W = 0 \tag{5}$$

In the above equations, W represents the catalyst mass, F_i and R_i are the molar inlet flow rate and the net production rate of the component i, respectively. The net rate of R of each component is defined as the total sum of the formation and consumption of each component.

$$R_i = \sum_j \nu_{ij} r_j \tag{6}$$

where ν_{ij} is the stoichiometric coefficient of component i in reaction j.

Since H_2 is in stoichiometric excess with respect to anisole, the change in the flow rate of H_2 was not considered in the analysis. The rate constants for the different reactions was determined by fitting the output flow rate of all components from Fig. 1 to the output of the system of ODEs in Eq. (4) in MATLAB® using lsqcurvefit function (detailed analysis given in Supplementary Note 2).

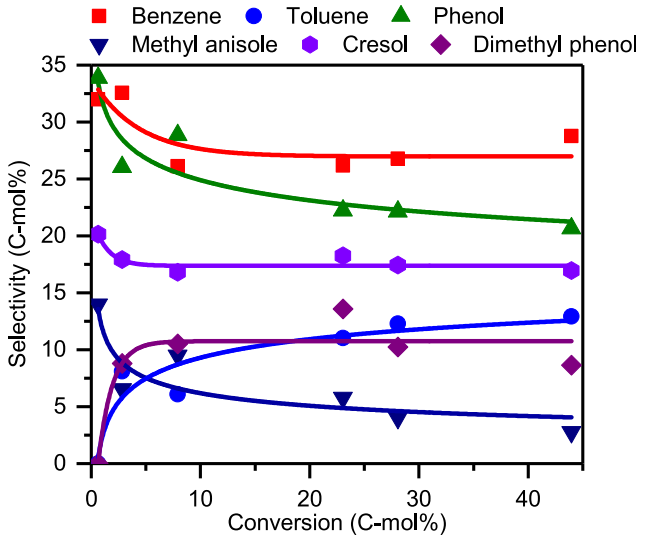

Fig. 1. . Selectivity of major products as a function of conversion of anisole on 10 wt% MoO_3/ZrO_2 catalyst. The selectivity is defined based on the carbon moles included in aromatic carbons. Cresol is mainly o-cresol. Reaction conditions: 1.5–150 mg of 10 wt% MoO_3/ZrO_2. P_{Total} = 1.013 bar (0.0098 bar $P_{Anisole}$, balance H_2). Temperature = 593 K. The solid trend lines serve as a guide to the eye. No other products were detected at the lowest three conversion values.

2.6. Thermodynamic calculations

The free energies for the reaction network at 593 K were calculated using the Gaussian 03 software [34]. The geometry and the energies were computed at the CBS-QB3 level of theory, using the rigid rotor harmonic oscillator approximation.

3. Results

3.1. Physicochemical properties of 10 wt% MoO_3/ZrO_2

The physicochemical properties of the catalyst including BET surface area, oxygen uptake, percentage of redox-active species and acid site concentration are summarized in Table 1. The percent of redox-active surface species was 31% as determined from oxygen chemisorption data. The acid site concentration was ~685 μϖ mol/g from NH_3-TPD data. At 10 wt% loading, the MoO_x domains on the ZrO_2 support are amorphous and oligomeric in nature [28]. The detailed physicochemical characterization of the catalysts of the MoO_3/ZrO_2 catalyst including the powder X-ray diffraction (PXRD) patterns and Raman spectra were reported in our previous studies [28].

3.2. Primary analysis of the products during anisole conversion

The primary and secondary products of anisole conversion were determined by plotting product selectivities as a function of conversion (0.6–44.0 C-mol %) at a temperature of 593 K, a $P_{Anisole}$ = 0.0098 bar, and a P_{H2} = 1.0032 bar (Fig. 1). Extrapolating product selectivity values of the major products to 0% conversion showed that benzene, phenol, cresol and methyl anisole are the primary aromatic products formed from anisole conversion (see Scheme 1). We note that the higher alkylated aromatics and oxygenates were formed at high conversions (Scheme 2 and Fig. S2). This product distribution suggests selective hydrodeoxygenation (HDO) of the O-$C_{aromatic}$ bond to form benzene, hydrogenolysis of the O-$C_{aliphatic}$ bond to form phenol, methyl migration from anisole to form cresol, and the alkylation of anisole to form methyl anisole. The latter product can be formed via intermolecular methyl migration, as suggested by Resasco and coworkers [35,36], intramolecular methyl migration, or secondary alkylation from surface methoxy species. The negative free energies for the individual reactions presented in Scheme 1 show that none of the primary reactions are equilibrium limited at the reaction conditions investigated. Although benzene and CH_3OH should be primary HDO products, CH_4 rather CH_3OH than was detected, suggesting that the HDO of methanol to methane is very fast at these conditions. We note the bare ZrO_2 support was active for the hydrogenolysis and alkylation reactions to form phenol, cresols and methyl anisole, albeit at rates ~2–3 lower than MoO_3/ZrO_2 (see Table S5) but was inactive for HDO to form benzene [33].

3.3. Kinetic analysis of primary product formation

Steady-state kinetics for the formation of primary products were obtained under differential conditions in the absence of external and internal mass-transfer limitations as determined by meeting the Mears and Weisz-Prater criteria, respectively (see Supplementary Note 1). ZrO_2 were used in addition to the 10 wt% MoO_3/ZrO_2 catalyst in order to gain insights into the effects of the support.

3.3.1. Apparent reaction orders for benzene production

The benzene formation rate for the 10 wt% MoO_3/ZrO_2 catalyst exhibited a near zero-order dependence (−0.03 ± 0.08) with $P_{Anisole}$

Table 1
Textural properties, oxygen chemisorption values and acid site concentration from NH_3-TPD for 10 wt% MoO_3/ZrO_2 catalyst.

Catalyst	BET surface area (m^2/g)	Mo density (Mo/nm^2)	Oxygen uptake (μmol/g)	% redox-active species	Acid-site concentration (μmol/g)
10 wt% MoO_3/ZrO_2	112	3.7	107	31	685

Oxygen uptake and % redox-active species were reported from Shetty et al. [33]. The catalyst was reduced at 623 K for 2 h and oxygen uptake was measured at 303 K.

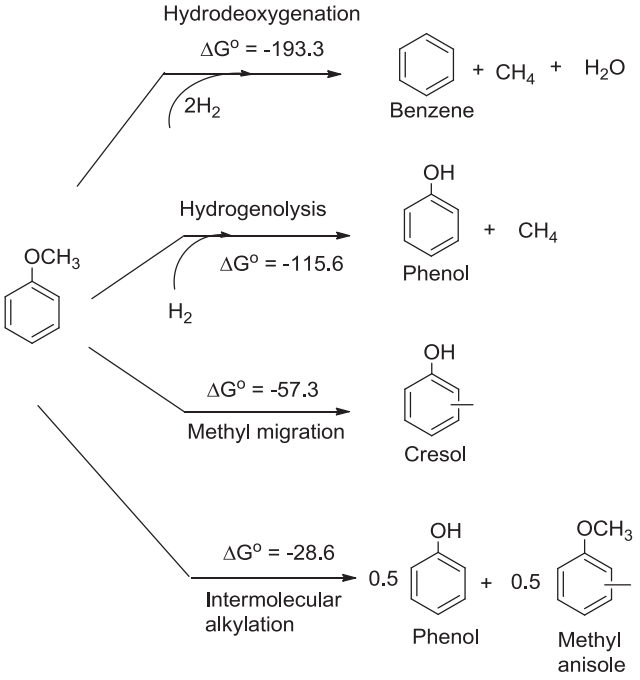

Scheme 1. Free energy values for the primary reaction pathways and their corresponding products from anisole conversion. All the free energy values are reported in units of kJ mol^{-1} in the gas phase at 593 K.

(Fig. 2a). Benzene formation rates from phenol were also near zero-order (0.02 ± 0.08) with respect to P_{Phenol}. These data are consistent with previous reports of HDO rates of m-cresol and anisole on supported MoO_3 and bulk Mo_2C catalysts [28,37].

The rate of benzene production from anisole and phenol exhibited apparent first-order (0.96 ± 0.03) and half order (0.54 ± 0.03) dependencies, respectively, on P_{H2} (Fig. 2b). An apparent half-order (0.56 ± 0.05) with respect to P_{H2} was also observed for the HDO of m-cresol to toluene (Fig. S3). The apparent activation energy for anisole HDO was 116 ± 2 kJ mol^{-1} in the temperature range of 573–613 K, while phenol featured an apparent barrier of 98 ± 3 kJ mol^{-1} in the same temperature range (Fig. 2c). The difference in the reaction order with P_{H2} and apparent activation energies for the two HDO reactions implicates differences in the number of H additions prior to the rate determining step (RDS) in the HDO mechanism for each substrate (*vide infra*).

3.3.2. Apparent reaction orders for hydrogenolysis and alkylation on 10 wt% MoO_3/ZrO_2 catalyst and ZrO_2

Fig. 3 illustrates the dependence of phenol, cresol and methyl anisole formation rates on $P_{Anisole}$ and P_{H2} on the 10 wt% MoO_3/ZrO_2 catalyst. Phenol, cresol and methyl anisole formation rates showed orders with respect to $P_{Anisole}$ of 0.72 ± 0.06, 0.55 ± 0.09 and 0.43 ± 0.03, respectively. With varying P_{H2}, phenol, cresol, and methyl anisole formation rates showed orders of 0.48 ± 0.06, 0.71 ± 0.03 and 0.43 ± 0.03, respectively. The apparent activation energy barriers for phenol, cresol and methyl anisole formation from anisole were 93 ± 16, 100 ± 25 and 89 ± 21 kJ mol^{-1}, respectively, in the temperature range 573–633 K (Fig. S5).

The rates of phenol, cresol and methyl anisole formation increased ~2–3 times on MoO_3/ZrO_2 as compared to ZrO_2 support, as shown in Table S5 when normalized to the mass of ZrO_2. Therefore, the sites on the ZrO_2 support do not appear to play a dominant role towards the formation of oxygenates. The ZrO_2 support featured phenol, cresol and methyl anisole reactions orders of 1.2 ± 0.2, 1.2 ± 0.2, and 1.0 ± 0.2, respectively, with $P_{anisole}$ and near half-order with P_{H2} (Fig. S6). These values suggest the contribution of bimolecular pathways on the support for anisole conversion to phenol and cresol, leading to reaction orders greater than 1. The apparent activation energy for phenol formation from anisole on ZrO_2 was 85 ± 12 kJ mol^{-1} in the temperature range 573–613 K (Fig. S7), similar to MoO_3/ZrO_2. In contrast to bare ZrO_2, the apparent reaction orders with respect to anisole for MoO_3/ZrO_2 were all <1 with $P_{Anisole}$ suggesting that the coverages of surface species over the sites responsible for catalyzing these reactions in both the catalyst and the bare support are different (Supplementary Note 4).

3.4. Co-feed studies to determine the nature of active sites on 10 wt% MoO_3/ZrO_2

The nature of the active sites for the HDO, hydrogenolysis and alkylation reactions was interrogated with the aid of co-feed studies. Co-feeds that selectively inhibit product formation are useful for developing insights into the site-requirements for catalysis that are consistent with the kinetic studies. We note that the co-feeds were largely reversible adsorbates and were not used for quantitation. However, the reactions were not equilibrium limited as noted earlier, hence the co-feeds are not expected to appreciably affect the reaction equilibrium. Under our reaction conditions, H_2 is present in stoichiometric excess as compared to the oxygenate feed (usually anisole). Introduction of a co-feed (H_2O, pyridine and ditertbutyl pyridine) without change in the concentration of oxygenate leads to a negligible change in the P_{H2}. Thus, any change in reactivity can be attributed to the presence of the co-feed. CH_3OH was added in excess (P_{CH3OH} = 0.16 bar, $P_{CH3OH}/P_{anisole} \approx 16$) and alters the kinetics, effectively blocking many sites, and putting more methyl groups on the surface than regular anisole conversion.

3.4.1. Co-feed with H_2O co-feed during anisole conversion

Fig. 4 shows the impact of H_2O on the product distribution during anisole conversion over 10 wt% MoO_3/ZrO_2. First, anisole (0.0098 bar $P_{anisole}$) mixed with H_2 was introduced into the reactor. After ~1.2 h on stream, 0.032 bar P_{H2O} ($P_{H2O}/P_{Anisole} \approx 3$) was co-fed, leading to a decrease in HDO product (i.e., benzene and toluene) yields from ~8.8 and 3.6% to 1.6 and 0.7%, respectively, which corresponds to an 80% reduction on a C-mol basis. Note that at identical yields without the H_2O co-feed, the $P_{H2O}/P_{Anisole} \approx 0.15$, which indicates that inhibition by H_2O was limited under normal conditions. This inhibition effect was reversible, as shown by the fast recovery of the original yields when the water co-feed was stopped. A similar behavior was observed during the HDO of phenol and m-cresol in the presence of a H_2O co-feed (Figs. S9 and S10). Although the HDO activity was decreased, the presence of H_2O during anisole HDO increased the yields of other oxygenate products. For instance, phenol and cresol increased from 12.5

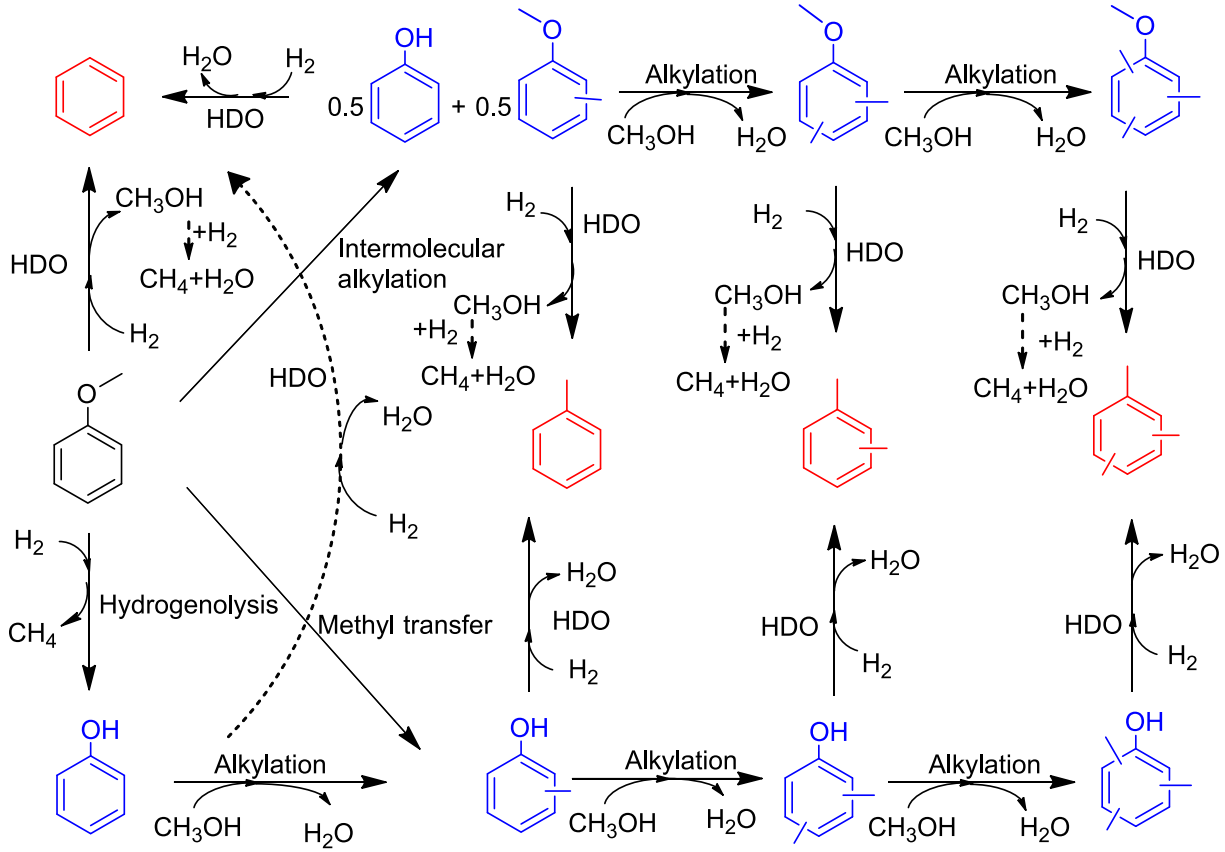

Scheme 2. Reaction network for anisole conversion for hydrodeoxygenation (HDO), hydrogenolysis, intra- and intermolecular alkylation reactions.

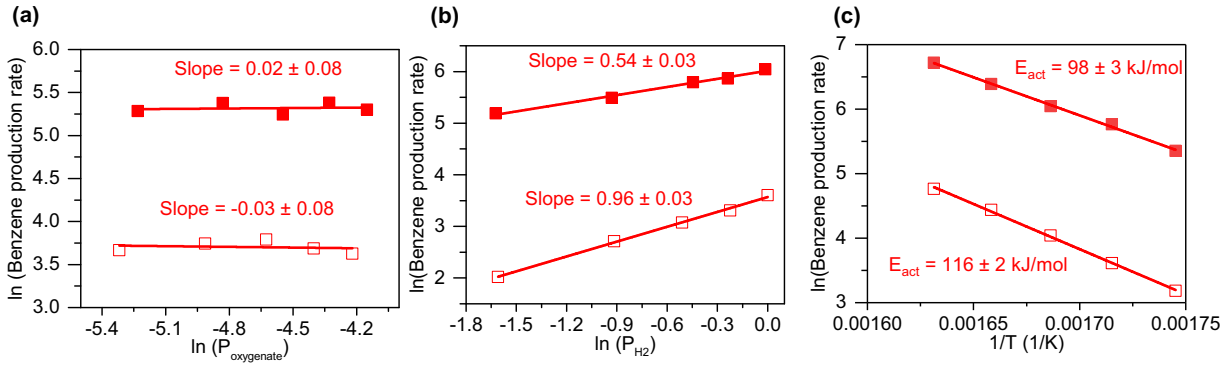

Fig. 2. Steady-state kinetic studies for anisole (open symbols) and phenol (closed symbols) HDO to benzene. The figure shows benzene production rates as a function (a) anisole and phenol partial pressure, (b) hydrogen partial pressures (P_{H2}), and (c) inverse temperature (1/T). Reaction conditions: (a) 25–30 mg MoO_3/ZrO_2. P_{Total} = 1.013 bar (0.0049–0.0147 bar $P_{Anisole}$ for anisole HDO, 0.0053–0.0155 bar P_{Phenol} and 0.0082–0.0244 $P_{mesitylene}$ for phenol HDO, balance H_2, temp = 593 K). (b) 30–40 mg MoO_3/ZrO_2. 0.0098 bar $P_{Anisole}$ and 0.2508–1.0032 bar P_{H2} for anisole HDO; 0.0106 bar P_{Phenol}, 0.0164 bar $P_{mesitylene}$ and 0.1972–0.986 bar P_{H2} for phenol HDO, balance N_2, temp = 593 K. (c) 30–40 mg MoO_3/ZrO_2. P_{Total} = 1.013 bar (0.0098 bar $P_{Anisole}$ for anisole HDO, 0.0106 bar P_{Phenol} and 0.0164 bar $P_{mesitylene}$ for phenol HDO, balance H_2), T = 573–613 K. The reaction rate is represented in mmol C h^{-1} g^{-1}_{MoO3}. The conversions were less than 15 C-mol% for all experiments.

and 9.9% to 24.5 and 15.5%, respectively. This effect was also observed during anisole conversion on the bare ZrO_2 support, as shown in Fig. S11 for an experiment using ~8 times more material.

3.4.2. Alkylation with CH_3OH co-feed during phenol HDO

In order to understand the role of methoxy species on oxygenate conversion, CH_3OH was co-fed at a concentration of P_{CH3OH} = 0.16 bar during phenol HDO over 10 wt% MoO_3/ZrO_2 (Fig. 5). At a TOS = 4 h, a co-feed of CH_3OH was introduced without altering the value of $P_{Anisole}$ (resulting in a $P_{CH3OH}/P_{Anisole} \approx 16$). The benzene yield decreased to almost zero, with a concomitant increase in CH_4 production (~5 mol% conversion of CH_3OH), indicating competitive adsorption of CH_3OH on the HDO sites. Further, the introduction of the CH_3OH co-feed resulted in the formation of alkylated products including cresol and dimethyl phenol with yields of ca. 10% and 5%, respectively, on a C-mol% basis of phenol fed. Similar effects were observed when CH_3OH was co-fed during m-cresol HDO (Fig. S12). No alkylated products were observed for a co-feed of CH_3OH with benzene, suggesting the adsorption of phenol through the O atom is critical for alkylation reactions to occur.

3.4.3. Co-feed with pyridine and DTBP

In order to further investigate the nature of active sites responsible for anisole conversion, we performed co-feed experiments

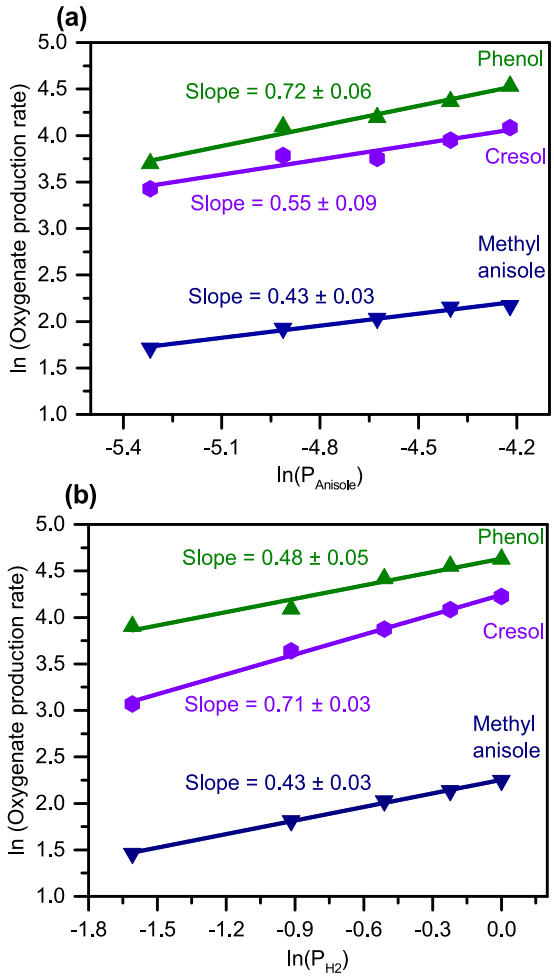

Fig. 3. Steady-state kinetic studies for anisole conversion to phenol, cresol and methyl anisole with respect to (a) anisole and (b) hydrogen concentrations. Reaction conditions: 30 mg MoO_3/ZrO_2. P_{Total} = 1.013 bar (0.0049–0.0147 bar $P_{Anisole}$, balance H_2, T = 593 K for a and 0.0098 bar $P_{Anisole}$, 0.2508–1.0032 bar P_{H2} with balance N_2 when P_{H2} < 1.0032 bar for (b). The reaction rate has units of mmol C h^{-1} g^{-1}_{MoO3}.

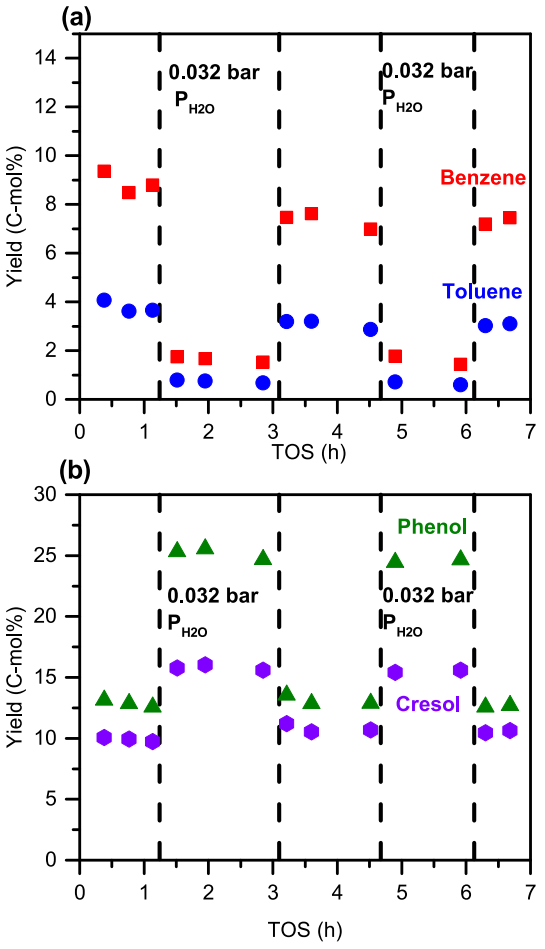

Fig. 4. Yield of benzene, toluene, phenol and cresol with and without co-feed of H_2O (0.032 bar P_{H2O}). Reaction conditions: 150 mg 10 wt% MoO_3/ZrO_2. P_{Total} = 1.013 bar (0.0098 bar $P_{Anisole}$, balance H_2 in the absence of H_2O co-feed. 0.0098 bar $P_{Anisole}$, 0.032 bar P_{H2O}, balance H_2 with H_2O co-feed). Temperature = 593 K.

with pyridine, a molecule that binds both to Lewis and Brønsted acid sites, and DTBP, a molecule that binds only to Brønsted acid sites [38]. As shown in Fig. 6, the pyridine co-fed ($P_{pyridine}$ = 0.0015 bar), decreased the yields of both HDO and oxygenate products, suggesting titration of sites responsible for HDO, hydrogenolysis, and alkylation. Benzene and cresol selectivity values changed from 28 and 16%, to 39% and 11%, respectively (Fig. S13). In contrast to the H_2O co-feed experiments, the original activity was not completely recovered after removing the pyridine (~30% as compared to 45% prior to pyridine introduction), yet the product distribution was not altered (Fig. S13). Pyridine co-feed during phenol HDO showed similar results (Fig. S14).

The role of Brønsted acid sites for HDO was tested by introducing a co-feed of DTBP (P_{DTBP} = ~0.0015 bar) during anisole and phenol HDO reactions. The bulky tert-butyl groups prevent DTBP from binding to Lewis acid sites due to steric effects, but do not prevent protonation by Brønsted acid sites [38]. As shown in Fig. 7, the DTBP co-feed led to a negligible reduction in benzene and toluene yields, which is in contrast to the results obtained with pyridine. Minimal reduction in hydrogenolysis/alkylation activity was observed in the presence of DTBP for anisole conversion. Specifically, the phenol, cresol, dimethyl phenol yield values decreased from 6.0 to 4.8, 4.5 to 3.8, and 3.0 to 2.5%, respectively. Similar results were obtained for phenol HDO (Fig. S15).

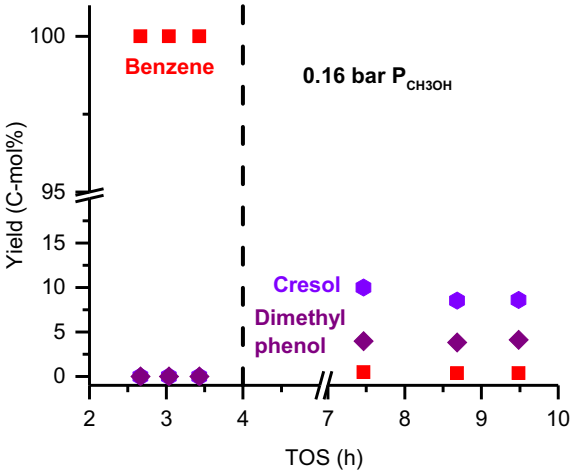

Fig. 5. Yield of benzene, cresol and dimethyl phenol from phenol with and without co-feed of methanol (~0.16 bar P_{CH3OH}). The basis is the carbon moles of phenol fed. Reaction conditions: 200 mg MoO_3/ZrO_2. P_{Total} = 1.013 bar (0.005 bar P_{Phenol}, 0.015 bar $P_{mesitylene}$, balance H_2 in the absence of CH_3OH co-feed. 0.005 bar P_{Phenol}, 0.16 bar P_{CH3OH}, 0.015 bar $P_{mesitylene}$, balance H_2 with CH_3OH co-feed). Temperature = 593 K. 25 wt% phenol solution in mesitylene.

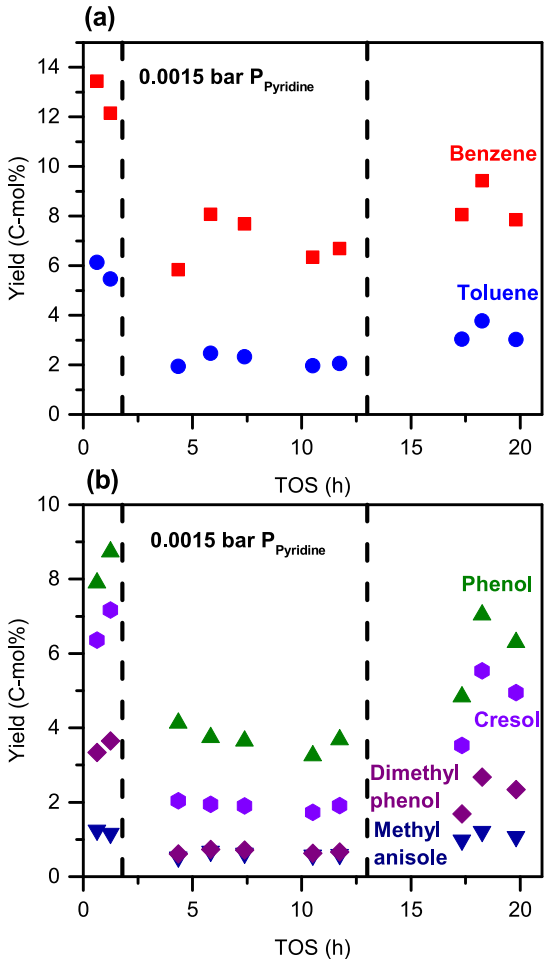

Fig. 6. Yield of HDO products benzene, toluene, and oxygenate products phenol, cresol, dimethyl phenol and methyl anisole with and without co-feed of pyridine (~0.0015 bar $P_{pyridine}$). Reaction conditions: 150 mg 10 wt% MoO_3/ZrO_2. P_{Total} = 1.013 bar (0.0098 bar $P_{Anisole}$, balance H_2 in the absence of pyridine co-feed. 0.0098 bar $P_{Anisole}$, 0.0015 bar $P_{pyridine}$, balance H_2 with pyridine co-feed). Temperature = 593 K.

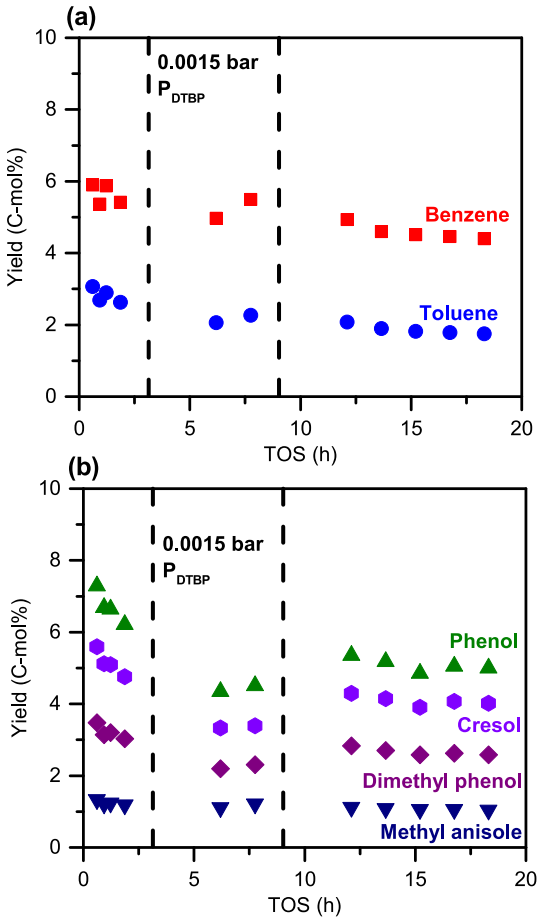

Fig. 7. Yield of HDO products benzene, toluene, and oxygenate products phenol, cresol, dimethyl phenol and methyl anisole with and without co-feed of DTBP (~0.0015 bar P_{DTBP}). Reaction conditions: 100 mg 10 wt% MoO_3/ZrO_2. P_{Total} = 1.013 bar (0.0098 bar $P_{Anisole}$, balance H_2 in the absence of DTBP co-feed. 0.0098 bar $P_{Anisole}$, 0.0015 bar P_{DTBP}, balance H_2 with DTBP co-feed). Temperature = 593 K.

To analyze the effect of reaction temperature on the adsorption of pyridine and DTBP on the catalyst surface, thermal treatment of the catalyst at 623 K was carried out after pyridine and DTBP adsorption and the FTIR spectra were analyzed. As shown in Fig. S16c and S16d, the bands at 1530 and 1615 cm^{-1} corresponding to DTBP adsorption weaken post the thermal treatment. The bands corresponding to both Lewis and Brønsted acid sites for pyridine (1440, 1490, 1530, 1575, 1610 and 1640 cm^{-1}) reduced in intensity post thermal treatment at 623 K. However, the reduction in the intensity was not as significant as that seen for DTBP (Figs. S16a and S16b).

4. Discussion

Reaction network analyses have been used to obtain mechanistic insights on reaction pathways, nature of active sites, and support effect on reactivity [18,35,36,39–44]. An analogous reaction network analyses for anisole conversion demonstrate the bifunctional nature of molybdenum supported on zirconia catalysts for catalyzing HDO, hydrogenolysis and alkylation reactions (Scheme 2). Indeed, previous studies on anisole deoxygenation and alcohol dehydration have shown that MoO_3/ZrO_2 feature both redox and acid sites [33,45–47]. Anisole is primarily converted to benzene by selective HDO, phenol by hydrogenolysis, cresol by a methyl transfer reaction, and methyl anisole by intermolecular alkylation. All the primary products can undergo sequential alkylation and/or HDO to form alkylated cresols, anisoles and benzenes, with the exception of deoxygenated aromatics which cannot be subsequently alkylated. A simplified kinetic model fitted for the data in Fig. 1 (details in Supplementary Note 2) showed that although the secondary pathway of phenol HDO to benzene has a rate constant ~ 3 times higher than that for the HDO of anisole to benzene, the anisole HDO pathway is dominant at low anisole conversions (<15 C-mol%).

Overall, our kinetic and co-feed studies suggested the involvement of active sites with a Lewis acid character for HDO [27,28,33,48], consistent with our previously hypothesized pathway driven by oxygen vacancies [26–28]. An apparent zero order dependence on oxygenate concentration suggests that oxygenate intermediates fully cover the oxygen vacancy sites at the reaction conditions. We hypothesize that H_2O and pyridine block these oxygen vacancies and we posit that the drastic reduction of benzene formation in the presence of CH_3OH is due to the surface coverage of HDO sites with methanol-derived intermediates.

The differences in reaction orders for oxygenate formation in relation to HDO indicate that the activation of oxygenates toward either HDO or hydrogenolysis/alkylation must occur on different sites. The lower activation energy for phenol formation via hydrogenolysis on both the 10 wt% MoO_3/ZrO_2 and ZrO_2 as compared to benzene formation via HDO further supports this hypothesis. We reason that the hydrogenolysis and alkylation reactions

are catalyzed by acid sites, as these sites are blocked by pyridine but cannot be blocked to a significant extent neither by H_2O, CH_3OH nor DTBP at the reaction conditions investigated and are enhanced in the presence of H_2O. Rather than promoting $C_{aromatic}$-O cleavage, these sites catalyze hydrolysis of the O-$C_{aliphatic}$ bond, generating CH_3OH in the presence of H_2O [35,36]. The hydrolysis increased the rates of phenol and cresol formation by ~2 times (Fig. 4) when using a 20-fold increase in P_{H2O} (with 40% conversion of anisole as reference). Given that H_2O is a byproduct of anisole HDO, it may explain contribution towards a small amount of phenol and cresol observed. Under differential conditions (<15% conversion), the contribution of water-promoted hydrolysis would be less than 2%. Therefore, the measured kinetics under differential conditions are likely not significantly influenced by the presence of H_2O due to HDO of anisole. In turn, CH_3OH readily alkylates the aromatic oxygenates, but not the deoxygenated arenes, suggesting the activation of the oxygenate through the O atom is critical for alkylation, consistent with a report by Anderson et al. on Mo-based polyoxometallates that feature both Lewis and Brønsted acid sites [12]. We note that this pathway is different from metal catalyzed hydrogenolysis of O-$C_{aliphatic}$ bonds [36,49].

We first consider a mechanism for phenol conversion to benzene (Table 2). This is comparatively easier to interpret due to the absence of alkylation and hydrogenolysis reactions. The experimental data strongly indicate that H_2 dissociation and HDO occur on two distinct sites: (*) and (S_2), respectively. On pre-reduced MoO_3/ZrO_2 (70 ml min^{-1} of 1.013 bar P_{H2} at 593 K for 1 h), only trace amounts of cyclohexane was observed at both 523 and 593 K when ~0.01 bar $P_{Benzene}$ was fed, suggesting very few metal sites are present at reaction conditions. While we cannot fully rule out the presence and influence of metallic sites for H_2 dissociation, it is also plausible that the sites responsible for H_2 activation could be undercoordinated Mo or Zr (for MoO_3/ZrO_2) moeities. Recent experimental and computational studies on CeO_2-ZrO_2 and RuO_2 have established that oxides can activate H_2 with an energy barrier less than 100 kJ mol^{-1} [50,51], which is within the range of observed activation energies in our current study. We posit that one H addition occurs on adsorbed phenol (Ph) prior to the rate-determining step (RDS, R4). With the assumption that the most abundant reactive intermediate (MARI) on S_2 is Ph-S_2, a reaction rate expression with 0 and 0.5 reaction order with respect to P_{phenol} and P_{H2}, respectively, is obtained (Supplementary Note 4).

The formation of benzene (Bz) from phenol (Ph) is found to be represented as given in Equation (7) below. A similar reaction rate expression can be obtained with the assumption of the H* addition to Ph-S_2 as the RDS.

$$r_{Phenol\rightarrow Benzene} = k_4 K_3 \sqrt{K_1 P_{H2}} \quad (7)$$

The HDO of anisole to benzene is complicated. The HDO, hydrogenolysis and alkylation reactions occur at comparable rates, and their measurements are affected by secondary reactions (Scheme 2). For example, CH_3 groups needed for alkylation are provided by HDO and hydrogenolysis, which exhibit different reaction orders. Our reaction kinetics and co-feed studies suggests that there are 3 distinct active sites responsible for H_2 dissociation (*), HDO (S_2) or hydrogenolysis/alkylation reactions (S_3). The P_{H2} dependencies on conversion of anisole to benzene and phenol to benzene are different, suggesting that either the RDS or H additions prior to the RDS, are different. One possibility is that anisole is first converted to phenol, followed by subsequent HDO of phenol to benzene. However, our analysis of the primary product selectivities with conversion (Fig. 1) suggests that this scenario is unlikely. Another possibility is that significant differences between -$OC_{aliphatic}H_3$ and –OH groups alter the barrier heights enough to change the dominant mechanism. Here, we show one possible mechanism consistent with our data, but we acknowledge other possibilities as shown in Supplementary Notes 4–6. Further work will be needed to fully elucidate the reaction mechanism.

In our model, molecular H_2 dissociatively adsorbs on the catalyst surface (*), while anisole (An) can adsorb on an oxygen vacancy (S_2), as suggested in our previous reports on bulk and supported MoO_3 catalysts [27,28]. We posit that the cleavage of the stronger $C_{aromatic}$-O bond (R8) occurs after two H addition. In this scheme, Reaction R8 is assumed to be the RDS with An-S_2 to be the MARI on S_2. This is similar with assumptions made by Bhan and coworkers on HDO reactions of oxygenates on Mo_2C catalysts [52]. We consider that both H* and CH_3* are mobile on the catalyst surface so that they can easily get to/from sites S_2 and S_3 to be involved in HDO and oxygenate formation. Hence, we suggest H* and CH_3* as surface intermediates on the catalyst surface without assigning to any particular site. This assumption was made to simplify the kinetic analysis. Finally, the site S_2 is regenerated with the release of H_2O.

The formation of benzene (Bz) from anisole (An) can be found to be represented by (Supplementary Note 4) Equation 10 as given below

$$r_{Anisole\rightarrow Benzene} = k_8 K_1 K_6 K_7 P_{H2} \quad (8)$$

Table 2
Elementary steps for hydrodeoxygenation (HDO) of phenol and anisole and formation of phenol, cresol and methyl anisole from anisole on MoO_3/ZrO_2.

Dissociative hydrogen adsorption		Anisole adsorption on S_3	
$H_2 + 2^* \leftrightarrow + 2H^*$	(R1)	An + $S_3 \leftrightarrow$ An - S_3	(R15)
Phenol HDO		**Phenol formation**	
Ph + $S_2 \leftrightarrow$ Ph - S_2	(R2)	An - S_3+$H^* \leftrightarrow$ $PhCH_3$ - S_3 + *	(R16)
Ph - S_2+ $H^* \leftrightarrow$ PhH - S_2 + *	(R3)	$PhCH_3$ - S_3 + $^* \overset{RDS}{\rightarrow}$ Ph - S_3 + CH_3^*	(R17)
PhH - $S_2 \overset{RDS}{\rightarrow}$ Bz + OH - S_2	(R4)	Ph - $S_3 \leftrightarrow$ Ph + S_3	(R18)
Anisole HDO		**Methyl anisole formation**	
An + $S_2 \leftrightarrow$ An - S_2	(R5)	An - S_3 + $CH_3^* \overset{RDS}{\rightarrow}$ MAH - S_3 + *	(R19)
An - S_2+ $H^* \leftrightarrow$ $PhCH_3$ - S_2 + *	(R6)	MAH - S_3 + $^* \leftrightarrow$ MA - S_3 + H^*	(R20)
$PhCH_3$ - S_2 + $H^* \leftrightarrow$ $BzOHCH_3$ - S_2 + *	(R7)	MA - $S_3 \leftrightarrow$ MA + S_3	(R21)
$BzOHCH_3$ - $S_2 \overset{RDS}{\rightarrow}$ Bz + CH_3OH - S_2	(R8)	**Cresol formation**	
CH_3OH - S_2 + $^* \rightarrow CH_3^*$ + OH - S_2	(R9)	Ph - S_3 + $CH_3^* \overset{RDS}{\rightarrow}$ CrH - S_3 + *	(R22)
CH_3OH - S_2 + $^* \leftrightarrow H^*$+ CH_3O - S_2	(R10)	CrH - S_3 + $^* \leftrightarrow$ Cr - S_3+ H^*	(R23)
CH_3^* + $H^* \rightarrow CH_4$ + 2*	(R11)	Cr - $S_3 \leftrightarrow$ Cr + S_3	(R24)
CH_3OH - $S_2 \leftrightarrow CH_3OH$ + S_2	(R12)		
OH - S_2+ $H^* \leftrightarrow H_2O$ - S_2 + *	(R13)		
H_2O - $S_2 \leftrightarrow H_2O$ + S_2	(R14)		

The formation of phenol on S_3 and benzene on S_2 from anisole can be hypothesized to be due to the difference in oxophilicity of the sites. The oxophilicity of the sites plays a role in adsorption of aromatic oxygenates by facilitating the adsorption through the oxygen atom and repulsion of phenyl ring with the catalyst surface [53]. Furthermore, it has been shown to reduce activation barriers for direct $C_{aromatic}$-O cleavage [49]. We hypothesize the oxophilic sites (S_2) in MoO_3/ZrO_2 play a similar role promoting the adsorption of anisole through the O atom and facilitates direct $C_{aromatic}$-O bond cleavage.

We assume the cleavage of the $C_{aliphatic}$-O bond (R17) and CH_3^* addition to An-S_3 (R19) and Ph-S_3 (R22) to be the RDS for phenol, methyl anisole and cresol formation, respectively. Due to the coupled nature of the reaction network, the exact reaction orders in the kinetic expressions of phenol, methyl anisole and cresol formation rates on MoO_3/ZrO_2 could not be derived. However, we note that these expressions correctly describe our kinetic data. The detailed derivations can be found in Supplementary Note 4. We further note that the kinetic rate expressions on ZrO_2 with decoupled HDO and oxygenate formation pathways are consistent with experimental data (Supplementary Note 4 through 6).

The presence of CH_3OH or H_2O leads to an increase in methoxy or hydroxyl species on S_2 (H_2O-S_2 and OH-S_2, or CH_3OH-S_2 or CH_3O-S_2), leading to a low coverage of intermediates from anisole or phenol and low HDO rates. When CH_3OH or H_2O is introduced with P_{H2O} and P_{CH3OH} significantly greater than $P_{Anisole}$, HDO is blocked and selectivities towards hydrogenolysis and alkylation are also significantly altered. The alkylation of phenol when CH_3OH is fed (R19 and R22) suggests that CH_3OH reacts through R9 leading to formation of CH_3^* species.

5. Conclusions

In summary, we carried out a comprehensive kinetic study for the vapor-phase anisole HDO over a 10 wt% MoO_3/ZrO_2 catalyst. Benzene, phenol, cresol and methyl anisole were confirmed as primary reaction products, while dimethyl phenol, toluene and dimethyl anisole, and the higher alkylated phenols, benzenes and anisoles were secondary and tertiary products, respectively. Co-feed and kinetic analyses suggested the involvement of distinct sites for the activation of anisole for HDO and for hydrogenolysis/alkylation. The kinetic models suggest that anisole is activated on an oxygen vacancy site with a Lewis acid character for HDO. The formation of deoxygenated products on an oxygen vacancy may be related to the oxophilicity of the undercoordinated surface. Our study paves the way for a molecular understanding of catalysis on bulk and supported molybdenum oxide catalysts for HDO.

Author contributions

The manuscript was written through contributions of all authors. All authors have given approval to the final version of the manuscript.

Declaration of Competing Interest

The authors declared that there is no conflict of interest.

Acknowledgment

This research was funded by BP through the MIT Energy Initiative Advanced Conversion Research Program. Eric Anderson acknowledges support by the National Science Foundation, CBET Award No 1454299.

Appendix A. Supplementary material

Supplementary data to this article can be found online at https://doi.org/10.1016/j.jcat.2019.06.046.

References

[1] G.W. Huber, S. Iborra, A. Corma, Synthesis of transportation fuels from biomass: chemistry, catalysts, and engineering, Chem. Rev. 106 (2006) 4044–4098.
[2] G.W. Huber, A. Corma, Synergies between bio- and oil refineries for the production of fuels from biomass, Angew. Chem. 46 (2007) 7184–7201.
[3] Q. Zhang, J. Chang, T. Wang, Y. Xu, Review of biomass pyrolysis oil properties and upgrading research, Energy Convers. Manag. 48 (2007) 87–92.
[4] T.R. Carlson, G.A. Tompsett, W.C. Conner, G.W. Huber, Aromatic production from catalytic fast pyrolysis of biomass-derived feedstocks, Top. Catal. 52 (2009) 241–252.
[5] E. Furimsky, Hydroprocessing challenges in biofuels production, Catal. Today 217 (2013) 13–56.
[6] A.J. Ragauskas, G.T. Beckham, M.J. Biddy, R. Chandra, F. Chen, M.F. Davis, B.H. Davison, R.A. Dixon, P. Gilna, M. Keller, P. Langan, A.K. Naskar, J.N. Saddler, T.J. Tschaplinski, G.A. Tuskan, C.E. Wyman, Lignin valorization: improving lignin processing in the biorefinery, Science 344 (2014).
[7] K. Wang, P.A. Johnston, R.C. Brown, Comparison of in-situ and ex-situ catalytic pyrolysis in a micro-reactor system, Bioresour. Technol. 173 (2014) 124–131.
[8] S. Van den Bosch, W. Schutyser, S.T. Renders, T. De Boe, S.F. Koelewijn, A. Dewaele, T. Ennaert, O. Verkinderen, B. Goderis, C.M. Courtin, B.F. Sels, Influence of bio-based solvents on the catalytic reductive fractionation of birch wood, Green Chem. 17 (2015) 5035–5045.
[9] S. Van den Bosch, W. Schutyser, S.F. Koelewijn, T. Renders, C.M. Courtin, B.F. Sels, Tuning the lignin oil OH-content with Ru and Pd catalysts during lignin hydrogenolysis on birch wood, Chem. Commun. 51 (2015) 13158–13161.
[10] S. Van den Bosch, W. Schutyser, R. Vanholme, T. Driessen, S.F. Koelewijn, T. Renders, B. De Meester, W.J.J. Huijgen, W. Dehaen, C.M. Courtin, B. Lagrain, W. Boerjan, B.F. Sels, Reductive lignocellulose fractionation into soluble lignin-derived phenolic monomers and dimers and processable carbohydrate pulps, Energy Environ. Sci 8 (2015) 1748–1763.
[11] E.M. Anderson, R. Katahira, M. Reed, M.G. Resch, E.M. Karp, G.T. Beckham, Y. Román-Leshkov, Reductive catalytic fractionation of corn stover lignin, ACS Sustain. Chem. Eng. 4 (2016) 6940–6950.
[12] E.M. Anderson, A. Crisci, K. Murugappan, Y. Roman-Leshkov, Bifunctional molybdenum polyoxometalates for the combined hydrodeoxygenation and alkylation of lignin-derived model phenolics, ChemSusChem (2017) 2226–2234.
[13] E.M. Anderson, M.L. Stone, R. Katahira, M. Reed, G.T. Beckham, Y. Román-Leshkov, Flowthrough reductive catalytic fractionation of biomass, Joule 1 (2017) 613–622.
[14] T. Iida, M. Shetty, K. Murugappan, Z. Wang, K. Ohara, T. Wakihara, Y. Roman-Leshkov, Encapsulation of molybdenum carbide nanoclusters inside zeolite micropores enables synergistic bifunctional catalysis for anisole hydrodeoxygenation, ACS Catal. (2017) 8147–8151.
[15] Q. Lu, C.J. Chen, W. Luc, J.G.G. Chen, A. Bhan, F. Jiao, Ordered mesoporous metal carbides with enhanced anisole hydrodeoxygenation selectivity, ACS Catal. 6 (2016) 3506–3514.
[16] E.M. Anderson, M.L. Stone, M.J. Hulsey, G.T. Beckham, Y. Roman-Leshkov, Kinetic studies of lignin solvolysis and reduction by reductive catalytic fractionation decoupled in flow-through reactors, ACS Sustain. Chem. Eng. 6 (2018) 7951–7959.
[17] M. Shetty, D. Zanchet, W.H. Green, Y. Román-Leshkov, Cooperative Co0/CoII sites stabilized by a perovskite matrix enable selective C–O and C–C bond hydrogenolysis of oxygenated arenes, ChemSusChem 12 (2019) 2171–2175.
[18] L. Nie, D.E. Resasco, Kinetics and mechanism of m-cresol hydrodeoxygenation on a Pt/SiO2 catalyst, J. Catal. 317 (2014) 22–29.
[19] K. Lee, G.H. Gu, C.A. Mullen, A.A. Boateng, D.G. Vlachos, Guaiacol hydrodeoxygenation mechanism on Pt(111): insights from density functional theory and linear free energy relations, ChemSusChem 8 (2015) 315–322.
[20] M.M. Sullivan, C.J. Chen, A. Bhan, Catalytic deoxygenation on transition metal carbide catalysts, Catal. Sci. Tech. 6 (2016) 602–616.
[21] M.J. Gilkey, C. Brady, D.G. Vlachos, B.J. Xuo, Characterization of oxidation states in metal/metal oxide catalysts in liquid-phase hydrodeoxygenation reactions with a trickle bed reactor, Ind. Eng. Chem. Res. 57 (2018) 5591–5598.
[22] C. Wang, A.V. Mironenko, A. Raizada, T. Chen, X. Mao, A. Padmanabhan, D.G. Vlachos, R.J. Gorte, J.M. Vohs, Mechanistic study of the direct hydrodeoxygenation of m-Cresol over WOx-Decorated Pt/C catalysts, ACS Catal. 8 (2018) 7749–7759.
[23] D.R. Moberg, T.J. Thibodeau, F.G. Amar, B.G. Frederick, Mechanism of hydrodeoxygenation of acrolein on a cluster model of MoO3, J. Phys. Chem. C 114 (2010) 13782–13795.
[24] D.H. Mei, A.M. Karim, Y. Wang, Density functional theory study of acetaldehyde hydrodeoxygenation on MoO3, J. Phys. Chem. C 115 (2011) 8155–8164.

[25] K. Murugappan, E.M. Anderson, D. Teschner, T.E. Jones, K. Skorupska, Y. Roman-Leshkov, Operando NAP-XPS unveils differences in MoO3 and Mo2C during hydrodeoxygenation, Nat. Catal. 1 (2018) 960–967.
[26] T. Prasomsri, T. Nimmanwudipong, Y. Roman-Leshkov, Effective hydrodeoxygenation of biomass-derived oxygenates into unsaturated hydrocarbons by MoO3 using low H2 pressures, Energy Environ. Sci. 6 (2013) 1732–1738.
[27] T. Prasomsri, M. Shetty, K. Murugappan, Y. Román-Leshkov, Insights into the catalytic activity and surface modification of MoO3 during the hydrodeoxygenation of lignin-derived model compounds into aromatic hydrocarbons under low hydrogen pressures, Energy Environ. Sci. 7 (2014) 2660–2669.
[28] M. Shetty, K. Murugappan, T. Prasomsri, W.H. Green, Y. Roman-Leshkov, Reactivity and stability investigation of supported molybdenum oxide catalysts for the hydrodeoxygenation (HDO) of m-cresol, J. Catal. 331 (2015) 86–97.
[29] S. Budhi, C. Mukarakate, K. Iisa, S. Pylypenko, P.N. Ciesielski, M.M. Yung, B.S. Donohoe, R. Katahira, M.R. Nimlos, B.G. Trewyn, Molybdenum incorporated mesoporous silica catalyst for production of biofuels and value-added chemicals via catalytic fast pyrolysis, Green Chem. 17 (2015) 3035–3046.
[30] K. Murugappan, C. Mukarakate, S. Budhi, M. Shetty, M.R. Nimlos, Y. Román-Leshkov, Supported molybdenum oxides as effective catalysts for the catalytic fast pyrolysis of lignocellulosic biomass, Green Chem. 5548–5557 (2016).
[31] M.W. Nolte, J. Zhang, B.H. Shanks, Ex situ hydrodeoxygenation in biomass pyrolysis using molybdenum oxide and low pressure hydrogen, Green Chem. 18 (2016) 134–138.
[32] G. Zhou, P.A. Jensen, D.M. Le, N.O. Knudsen, A.D. Jensen, Atmospheric hydrodeoxygenation of biomass fast pyrolysis vapor by MoO3, ACS Sustain. Chem. Eng. 4 (2016) 5432–5440.
[33] M. Shetty, K. Murugappan, W.H. Green, Y. Roman-Leshkov, Structural properties and reactivity trends of molybdenum oxide catalysts supported on zirconia for the hydrodeoxygenation of anisole, ACS Sustain. Chem. Eng. 5 (2017) 5293–5301.
[34] M.J. Frisch, Gaussian 03, Gaussian, 2004.
[35] X.L. Zhu, R.G. Mallinson, D.E. Resasco, Role of transalkylation reactions in the conversion of anisole over HZSM-5, Appl. Catal. A 379 (2010) 172–181.
[36] X.L. Zhu, L.L. Lobban, R.G. Mallinson, D.E. Resasco, Bifunctional transalkylation and hydrodeoxygenation of anisole over a Pt/HBeta catalyst, J. Catal. 281 (2011) 21–29.
[37] W.S. Lee, Z.S. Wang, R.J. Wu, A. Bhan, Selective vapor-phase hydrodeoxygenation of anisole to benzene on molybdenum carbide catalysts, J. Catal. 319 (2014) 44–53.
[38] C.D. Baertsch, K.T. Komala, Y.H. Chua, E. Iglesia, Genesis of Bronsted acid sites during dehydration of 2-butanol on tungsten oxide catalysts, J. Catal. 205 (2002) 44–57.
[39] T. Nimmanwudipong, R.C. Runnebaum, D.E. Block, B.C. Gates, Catalytic conversion of guaiacol catalyzed by platinum supported on alumina: reaction network including hydrodeoxygenation reactions, Energy Fuels 25 (2011) 3417–3427.
[40] T. Nimmanwudipong, R.C. Runnebaum, D.E. Block, B.C. Gates, Catalytic reactions of guaiacol: reaction network and evidence of oxygen removal in reactions with hydrogen, Catal. Lett. 141 (2011) 779–783.
[41] R.C. Runnebaum, R.J. Lobo-Lapidus, T. Nimmanwudipong, D.E. Block, B.C. Gates, Conversion of anisole catalyzed by platinum supported on alumina: the reaction network, Energy Fuels 25 (2011) 4776–4785.
[42] T. Nimmanwudipong, C. Aydin, J. Lu, R.C. Runnebaum, K.C. Brodwater, N.D. Browning, D.E. Block, B.C. Gates, Selective hydrodeoxygenation of guaiacol catalyzed by platinum supported on magnesium oxide, Catal. Lett. 142 (2012) 1190–1196.
[43] R.C. Runnebaum, T. Nimmanwudipong, D.E. Block, B.C. Gates, Catalytic conversion of compounds representative of lignin-derived bio-oils: a reaction network for guaiacol, anisole, 4-methylanisole, and cyclohexanone conversion catalysed by Pt/γ-Al2O3, Catal. Sci. Technol. 2 (2012) 113–118.
[44] R.C. Runnebaum, T. Nimmanwudipong, R.R. Limbo, D.E. Block, B.C. Gates, Conversion of 4-methylanisole catalyzed by Pt/γ-Al2O3 and by Pt/SiO2-Al2O3: reaction networks and evidence of oxygen removal, Catal. Lett. 142 (2012) 7–15.
[45] J. Macht, C.D. Baertsch, M. May-Lozano, S.L. Soled, Y. Wang, E. Iglesia, Support effects on Bronsted acid site densities and alcohol dehydration turnover rates on tungsten oxide domains, J. Catal. 227 (2004) 479–491.
[46] J. Xu, A.M. Zheng, J. Yang, Y.C. Su, J.Q. Wang, D.L. Zeng, M.J. Zhang, C.H. Ye, F. Deng, Acidity of mesoporous MoOx/ZrO2 and WOx/ZrO2 materials: a combined solid-state NMR and theoretical calculation study, J. Phys. Chem. B 110 (2006) 10662–10671.
[47] R.M. West, D.J. Braden, J.A. Dumesic, Dehydration of butanol to butene over solid acid catalysts in high water environments, J. Catal. 262 (2009) 134–143.
[48] M. Shetty, B. Buesser, Y. Román-Leshkov, W.H. Green, Computational Investigation on Hydrodeoxygenation (HDO) of acetone to propylene on α-MoO3 (010) surface, J. Phys. Chem. C 121 (2017) 17848–17855.
[49] Q.H. Tan, G.H. Wang, A. Long, A. Dinse, C. Buda, J. Shabaker, D.E. Resasco, Mechanistic analysis of the role of metal oxophilicity in the hydrodeoxygenation of anisole, J. Catal. 347 (2017) 102–115.
[50] S.M. Schimming, G.S. Foo, O.D. LaMont, A.K. Rogers, M.M. Yung, A.D. D'Amico, C. Sievers, Kinetics of hydrogen activation on ceria-zirconia, J. Catal. 329 (2015) 335–347.
[51] A.V. Mironenko, D.G. Vlachos, Conjugation-driven "Reverse Mars–van Krevelen"-type radical mechanism for low-temperature C-O bond activation, J. Am. Chem. Soc. 138 (2016) 8104–8113.
[52] A. Kumar, S. Phadke, A. Bhan, Acetic acid hydrodeoxygenation on molybdenum carbide catalysts, Catal. Sci. Technol 8 (2018) 2938–2953.
[53] P.M. de Souza, L. Nie, L.E.P. Borges, F.B. Noronha, D.E. Resasco, Role of oxophilic supports in the selective hydrodeoxygenation of m-cresol on Pd catalysts, Catal. Lett. 144 (2014) 2005–2011.